DOI: 10.1002/ejic.200700061

Tripodal Trimanganese(III) Complexes of New Unsymmetrical Pentadentate Ligands Derived from 2-(Salicylideneamino)phenol: Syntheses, Crystal Structures and Properties

Masahiro Muto,[a] Naoya Hatae,[a] Yumi Tamekuni,[a] Yasunori Yamada,[a] Masayuki Koikawa,*[a] and Tadashi Tokii*[a]

Keywords: Bridging ligands / Ligand design / Manganese / X-ray structures / Magnetic properties / Redox chemistry

Trinuclear manganese(III) complexes of new unsymmetrical pentadentate ligands, 6-hydroxy-2-(2-hydroxyphenyl)-5-(salicylideneamino)benzoxazole (H_3L^1) and 5-(5,6-benzosalicylideneamino)-6-hydroxy-2-(2-hydroxynaphthyl)benzoxazole (H_3L^2), $[Mn_3(L^1)_3(CH_3OH)_3]$ (**1**) and $[Mn_3(L^2)_3(dmf)(CH_3OH)(H_2O)]$ (**2**) (dmf = *N*,*N*-dimethylformamide), have been prepared. The structures of the ligands H_3L^1, H_3L^2 and complex **1** were determined by X-ray crystallography, which revealed that the ligands have two distant chelating sites. The molecular structure of **1** is regarded as a tripodal pyramid with a cavity of about 3 Å diameter. Each Mn^{III} ion is coordinated by *ONO* atoms from a tridentate Schiff base site and *ON* atoms from a benzoxazole site of two respective H_3L^1 ligands. The intramolecular Mn···Mn distances for **1** are in the range 8.0683–8.1791 Å, and the nearest intermolecular Mn···Mn distance, 5.7824(15) Å, is shorter than the intramolecular values. Magnetic measurements of **1** indicate that weak antiferromagnetic interactions ($J = -0.2\ cm^{-1}$, $g = 2.0$) are dominant in the trinuclear manganese(III) core. Cyclic voltammogram of **1** in dmf showed obscure redox couples assigned to two single-electron transfer processes.

Introduction

The development of nanoscale molecular architectures such as macrocyclic metal ion arrays is of considerable interest in materials science and supramolecular chemistry because these complexes often have characteristic redox, magnetic and mechanical functions and host–guest chemistry.[1–3] Moreover, the discrete macrocyclic structures can be used as secondary building units for higher-order constructions such as two- or three-dimensional network structures.[4,5] In any case, ligands that have appropriate bridging abilities and directions are used. For example, most macrocyclic metal complexes have been organised by small anions based on acetate and hydroxy anions. In this case, μ-acetato or μ-hydroxido bridges are slanted at small bending angles to the metal-to-metal direction. According to the extent of these angles, various sizes of macrocyclic metal arrangements are prepared. However, because the preparations of such complexes depend on contingency, it is rather difficult to strategically develop scientific research. Therefore, it is important that ligands that have multiple separate coordination sites, are carefully designed to obtain such nanomolecular architectures by self-assembly.

It is known that 2-(salicylideneamino)phenol (H_2sap)[6–11] and many other similar *ONO*-tridentate ligands form stable metal complexes.[12–20] We prepared modified ligands [H_3L^1: 6-hydroxy-2-(2-hydroxyphenyl)-5-(salicylideneamino)benzoxazole; H_3L^2: 5-(5,6-benzosalicylideneamino)-6-hydroxy-2-(2-hydroxynaphthyl)benzoxazole; H_4L': 4,6-bis(salicylideneamino)benzene-1,3-diol] and introduced *ON*-bidentate or *ONO*-tridentate coordination sites into H_2sap (Scheme 1). The newly designed ligands, H_3L^1 and H_3L^2, have unsymmetrical structures, and it is expected that H_3L^n will lead to polynuclear complexes that have a complicated structure because the two coordination sites face different directions. These unsymmetrical multidentate ligands can generally arrange metal ions suitable for the property of each coordination site. It is possible to apply the syntheses of functional models for metalloenzymes in the field of bioinorganic chemistry.[21–23] On the other hand, the symmetrical ligand H_4L', which has been known for a long time and was reported in detail in 1970,[24,25] is expected to lead to geometrically regularly structured complexes because it adapts *mer* coordination. Such symmetrical ligands are often used in studies of magnetism or electroconductivities, which require structural regularity.[25,26]

[a] Department of Chemistry and Applied Chemistry, Faculty of Science and Engineering, Saga University,
Honjo 1, Saga 840-8502, Japan
Fax: +81-952-28-8548
E-mail: koikawa@cc.saga-u.ac.jp

Supporting information for this article is available on the WWW under http://www.eurjic.org or from the author.

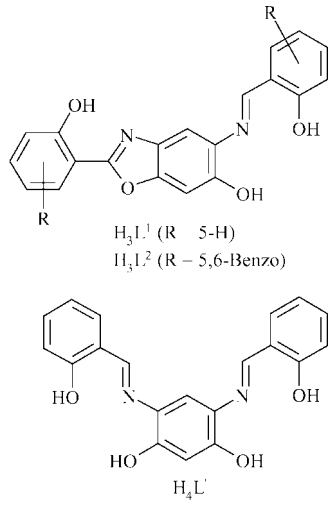

Scheme 1. Structure of the ligands.

In this study, we prepared new trinuclear manganese(III) complexes of these ligands with novel tripodal geometry. We describe here the syntheses, X-ray structural characterisation and magnetic and electrochemical properties of these newly obtained ligands and complexes.

Results and Discussion

The ligands H_3L^n and H_4L' were identified by elemental analysis, FTIR, ^{1}H NMR, FAB mass spectrometry and X-ray crystal structural analysis. The symmetrical ligand H_4L' was temporarily obtained as the monohydrochloride, H_4L'·HCl, from a simple reaction of 4,6-diaminoresorcinol dihydrochloride with 2-hydroxybenzaldehyde. This ligand showed characteristic IR bands assigned to ν(C=N) vibrations based on the Schiff base at 1622–1651 cm^{-1} and ν(OH) vibrations at 3070 and 3355 cm^{-1}. In the FAB mass spectrum, an intense molecular ion peak was observed at 349.1, and was assigned to the free ligand H_4L'. The free ligand H_4L' without HCl could be isolated when two equivalents of triethylamine were used in the synthetic process. These ligands, H_4L' and H_4L'·HCl, had similar ^{1}H NMR spectra. It is considered that both ligands have a comparable structure in solution. The unsymmetrical ligand H_3L^1 was prepared from the filtrate obtained in the synthetic process for free H_4L'. On the other hand, the homologous symmetrical ligand obtained using 2-hydroxy-1-naphthaldehyde was not isolated by a similar synthetic method for H_4L'. The unsymmetrical ligand H_3L^2 was obtained as a green product under basic reaction conditions with triethylamine. The starting material, 4,6-diaminoresorcinol, can be simply oxidised to *p*-quinone imine or *p*-semiquinone imine species. In fact, the intensity of an ESR signal related to the radical in crude 4,6-diaminoresorcinol gradually increases in air. It is supposed that symmetrical Schiff base ligands, the same as H_4L', are initially formed and that oxidation to a semiquinone imine form by molecular oxygen might have proceeded under such basic reaction conditions. Scheme 2 shows a reaction pathway for H_3L^1 formation. It is known that such radical species are stabilised by π conjugation as illustrated in Scheme 2. Consequently, the active radical species might lead to ring formation to yield benzoxazole derivatives. The free ligands H_3L^1 and H_3L^2 have characteristic IR bands assigned to ν(C=N) vibrations based on Schiff base and benzoxazoline components at 1615–1634 cm^{-1}, and ν(OH) vibrations at 3202 cm^{-1} for H_3L^1 and at 3051 cm^{-1} for H_3L^2. In the FAB mass spectra, intense molecular ion peaks were observed at 347.2 and 447.2.

The reaction of H_4L'·HCl and H_3L^2 with manganese(II) acetate tetrahydrate yielded trinuclear manganese(III) complexes **1** and **2**, respectively. Elemental analytical data of the complexes gave a 1:1 metal/ligand ratio. The ν(C=N) vibrations observed in free ligands shifted to about 1600 cm^{-1}. It is suggested that both binding sites act as tridentate and bidentate chelates. At ambient conditions the manganese(III) species are produced regardless of whether manganese(II) or manganese(III) is used as the manganese source. The formation of phenoxyl radicals as shown in Scheme 2 might be accelerated by the existence of manganese(III) species. As a result, it is supposed that H_4L' undergoes more facile oxidation to H_3L1 in these reactions. All attempts to obtain complex **1** by using H_3L^1 instead of

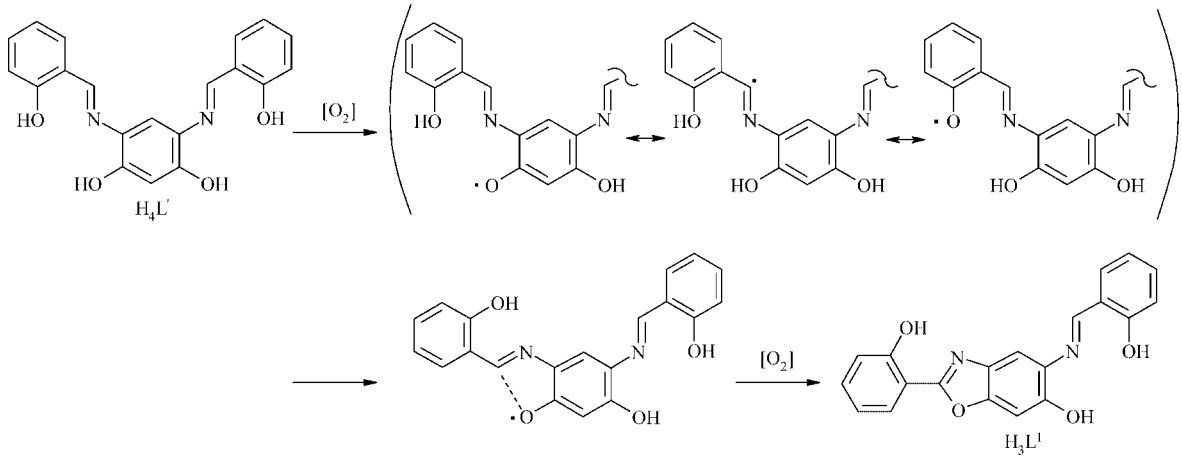

Scheme 2. Reaction pathway for the five-membered ring formation.

H_4L' were unsuccessful. One of the reasons was considered to be the low solubility of H_3L^1 in organic solvents.

X-ray Crystal Structures

Single crystals of H_4L', H_3L^1 and H_3L^2, suitable for X-ray crystallography, were obtained by recrystallisation from mixed dmf solution layered with methanol or acetonitrile. All the obtained crystals were thin and fragile needles. Although the structure refinements were insufficient, the obtained results clearly revealed the ligand structures. ORTEP drawings of these are shown in Figure 1. For ligand H_4L', both salicylaldehyde molecules formed Schiff base *ONO*-coordination sites such as 2-(salicylideneamino)phenol (H_2sap). On the other hand, H_3L^1 and H_3L^2 had *ON*-bidentate coordination sites comprising the benzoxazole substructure in addition to *ONO*-tridentate sites. The C(14)–N(2) bond length in H_3L^1 is 1.283(6) Å, and deviation of the five-membered ring, C(11)–C(12)–N(2)–C(14)–O(3), from planarity is very small (0.0060 Å). These data reveal the existence of a C=N double bond and the formation of a benzoxazole moiety, and prove that the ligand H_4L' can undergo facile oxidation in air. The molecular structures of H_3L^1 and H_3L^2 differ in planarity from H_2sap frameworks. As for the dihedral angles defined by two phenyl rings binding O(1) and O(2), the angles are 10.2(2)° (H_3L^1) and 4.9(4)° (H_3L^2). It is assumed that the H_2sap framework in H_3L^2 is much more delocalised than that in H_3L^1. In any case, *ON*- and *ONO*-coordination sites face opposite directions. Therefore, the ligand frameworks can be regarded to have an S-shape conformation (Table 1).

Table 1. Selected bond lengths and angles of **1**.

Bond lengths [Å]		Angles [°]	
Mn(1)–O(1)	1.895(5)	O(1)–Mn(1)–O(8)	91.3(2)
Mn(1)–O(2)	1.899(4)	O(1)–Mn(1)–N(1)	90.2(2)
Mn(1)–O(8)	1.901(5)	O(2)–Mn(1)–O(8)	94.9(2)
Mn(1)–O(13)	2.250(8)	O(2)–Mn(1)–N(1)	83.6(2)
Mn(1)–N(1)	1.989(6)	O(13)–Mn(1)–N(4)	173.1(2)
Mn(1)–N(4)	2.304(6)	O(5)–Mn(2)–O(12)	95.4(2)
Mn(2)–O(5)	1.916(5)	O(5)–Mn(2)–N(3)	88.7(2)
Mn(2)–O(6)	1.920(5)	O(6)–Mn(2)–O(12)	93.5(2)
Mn(2)–O(12)	1.874(5)	O(6)–Mn(2)–N(3)	82.4(2)
Mn(2)–O(14)	2.264(4)	O(14)–Mn(2)N(6)	171.0(2)
Mn(2)–N(3)	1.985(5)	O(4)–Mn(3)–O(9)	93.2(2)
Mn(2)–N(6)	2.241(6)	O(4)–Mn(3)–O(10)	93.1(2)
Mn(3)–O(4)	1.901(5)	O(9)–Mn(3)–N(5)	90.5(2)
Mn(3)–O(9)	1.895(5)	O(10)–Mn(3)–N(5)	83.3(2)
Mn(3)–O(10)	1.888(4)	O(15)–Mn(3)–N(2)	174.5(2)
Mn(3)–O(15)	2.241(8)		
Mn(3)–N(2)	2.250(6)		
Mn(3)–N(5)	2.000(5)		
Mn(1)···Mn(2)	8.1791(16)		
Mn(1)···Mn(3)	8.1081(15)		
Mn(2)···Mn(3)	8.0683(16)		

An ORTEP drawing of **1** is illustrated in Figure 2, and selected bond lengths and angles are listed in Table 2. The complex comprises three sets of ligands, manganese(III)

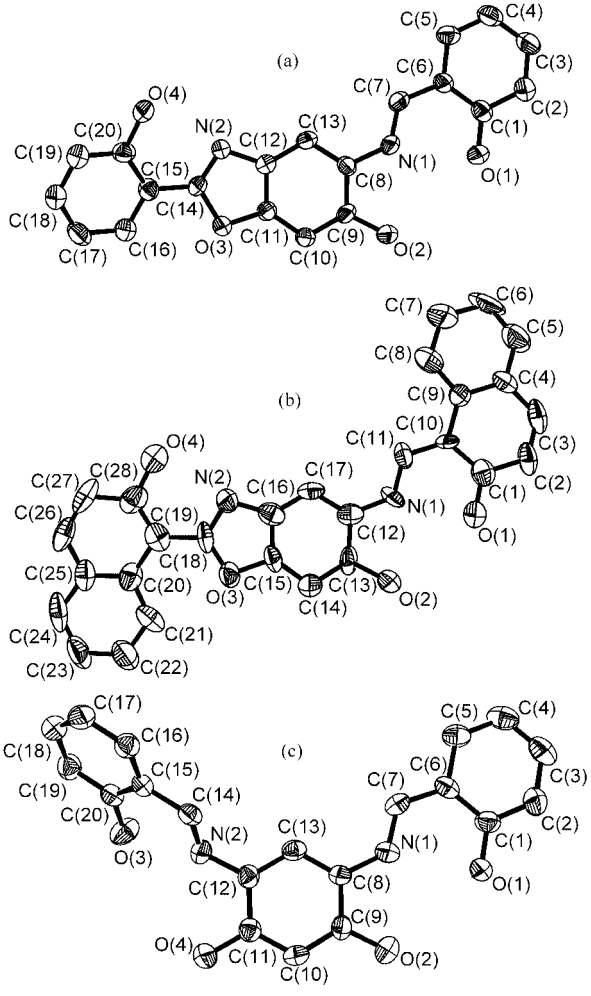

Figure 1. ORTEP drawings with the atom numbering scheme for the ligands; H_3L^1 (top), H_3L^2 (center) and H_4L' (bottom).

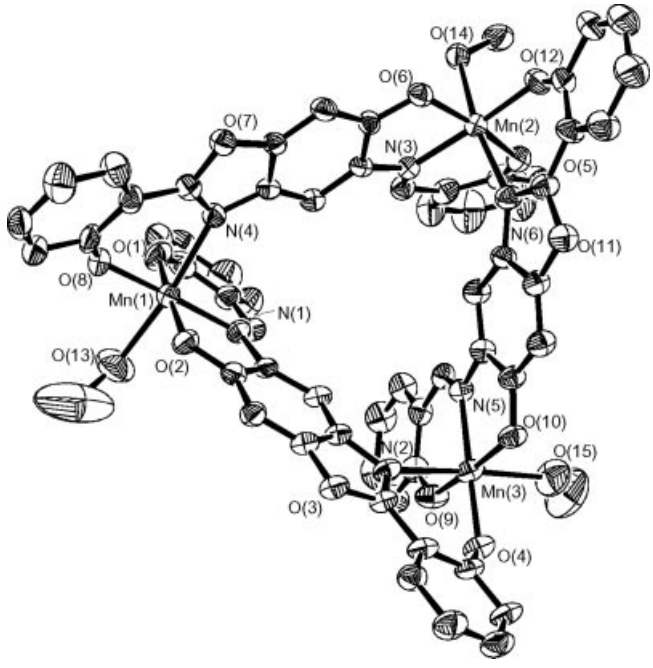

Figure 2. ORTEP view of **1** showing 30% probability.

Table 2. Electrochemical data of **1** and **2**.[a]

Complex	Mn_3(II,III,III)/Mn_3(II,II,III)			Mn_3(III,III,III)/Mn_3(II,III,III)			ΔE[c]
	E_{pa}	E_{pc}	$E_{1/2}(1)$[b]	E_{pa}	E_{pc}	$E_{1/2}(2)$[b]	
1	–0.68	–0.77	–0.73	–0.548	–0.64	–0.59	0.14
2	–0.70	–0.80	–0.75	–0.546	–0.71	–0.63	0.12

[a] In V vs. Ag/Ag^+, scan rate 100 $mV s^{-1}$. Determined on a GC electrode in dmf. [b] $E_{1/2} = (E_{pc} + E_{pa})/2$. [c] $\Delta E = |E_{1/2}(1) - E_{1/2}(2)|$.

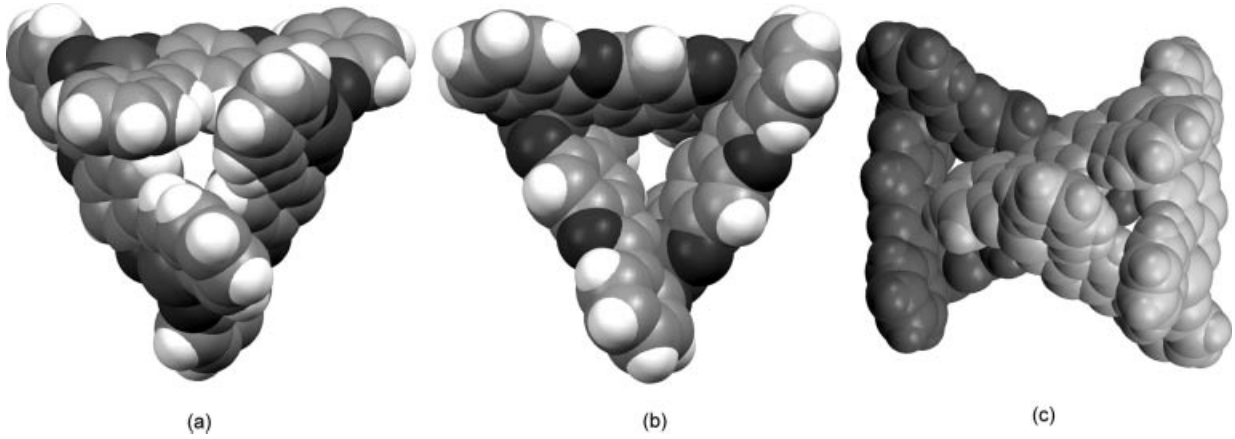

Figure 3. CPK models of **1**. Coordinating solvents are omitted for clarity; (a) view from the apex of the tripodal pyramid, (b) view from the cavity side and (c) enantiomer pairs in crystal packing; symmetry codes: (x, y, z) and ($1 - x$, $-y$, $1 - z$).

ions and coordinating solvents. CPK models of the $[Mn_3(L^1)_3]$ unit without the coordinating methanol molecules are shown in Figure 3. The entire molecular structure of **1** is regarded as a tripodal pyramid with a cavity. The coordination environments of the three manganese ions are very similar. Each manganese(III) ion forms a six-coordination geometry by three sets of donor components. The most effective donor set is the *ONO* one from the tridentate Schiff base binding site of $(L^1)^{3-}$. The N=C bond lengths (1.277–1.303 Å) in the Schiff base site are close to the value for standard $N(sp^2)=C(sp^2)$ double bonds. The sum of bond angles around N(1), N(3) and N(5) are 359.6, 359.3 and 359.8°, respectively. These data imply that the ligands are present in the Schiff base form, and not in the benzoxazine form. This coordination behaviour is very similar to that of 2-(salicylideneamino)phenol. The second one is the *ON* donor set from the bidentate benzoxazole site of a ligand different from the *ONO* donor. The phenolic oxygen atom coordinates to an identical plane, and the *ONO* Schiff base forms an equatorial plane. The nitrogen atom of the oxazole moiety is located in an axial position. The remaining sixth position of the manganese ion is occupied by a methanol molecule to form an $N_{oxazole}$–Mn–$O_{methanol}$ elongated axis. This axis corresponds to the Jahn–Teller axis for normal six-coordinate manganese(III) complexes. In complex **1**, the Jahn–Teller axes are defined as N(4)–Mn(1)–O(13) [Mn(1)–N(4) 2.304(6), Mn(1)–O(13) 2.250(8) Å], N(6)–Mn(2)–O(14) [Mn(2)–N(6) 2.241(6), Mn(2)–O(14) 2.264(4) Å] and N(2)–Mn(3)–O(15) [Mn(3)–N(2) 2.250(6), Mn(3)–O(15) 2.241(8) Å]. Equatorial planes comprise O(1)–N(1)–O(2)–O(8) for Mn(1) (av. 1.921 Å), O(5)–N(3)–O(6)–O(12) for Mn(2) (av. 1.924 Å) and O(9)–N(5)–O(10)–O(4) for Mn(3) (av. 1.921 Å). The bond lengths around the manganese(III) ions fall within the range observed for the manganese(III) complexes with Schiff base ligands.[16,27–31] In addition, coordination environments are very similar to that of [Mn(sap)L] [HL: 2-(2-hydroxyphenyl)benzoxazole], with a five-coordinate square-pyramidal structure, except for a coordinating methanol molecule.[17] It is well known that tridentate H_2sap derivatives usually form phenoxo-bridged dinuclear metal complexes.[6–9,18,20] However, when bidentate ligands such as phenanthroline are available, ternary mononuclear complexes such as [Mn(sap)L] are often reported.[11,19] In the present case, the reaction of H_3L^1 with manganese ions corresponds to the latter because H_3L^1 has both (sap) and bidentate coordination sites. As a result, H_3L^1 acts as an S-shaped hook to the manganese atom and locks each manganese atom to stabilise the tight triangular structure.

As for the characteristic structural properties, it is worth noting that these complexes have a cavity. The present complexes have long Mn···Mn distances arising from the unique ligand structure. The distances for **1** are 8.1791(16), 8.1081(15) and 8.0683(16) Å. Considering the van der Waals radius, a small molecule with an external diameter of about 3 Å can be held in the cavities. In fact, as shown in Figure 3, pairs of enantiomers are loosely aggregated in crystal lattices. In this pair, phenyl rings of the complexes are mutually intercalated in each cavity accompanied by π–π stacking [C(8)···$C(17)^i$ 3.411(10) Å]. It is suggested that these complexes can be expected in an application in host–guest chemistry. In the crystal packing, several intermolecular hydrogen bonds between coordinating solvents and neighbouring molecules are recognised. The distance be-

tween the O(14) atom of the coordinating methanol molecule and the O(8)^{j} atom of $(L^1)^{3-}$ in the neighbouring molecule is 2.949(7) Å, which is regarded as a typical hydrogen bond (symmetry code j: $1 - x$, $-1/2 - y$, $1/2 - z$). As a result, the nearest intermolecular Mn···Mn distance [Mn(2)···Mn(1)^{j} 5.7824(15) Å] is shorter than intramolecular Mn···Mn distances.

For complex **2**, X-ray reflection data and analytical results were insufficient for discussing structural details, because the crystals obtained were efflorescent. An identified molecular structure of **2** is very similar to that of **1** except for the coordinating solvent molecules. The estimated structure of **2** is consistent with the molecular formula suggested by the elemental analysis.

Magnetic Properties

Powder samples of the complexes showed two ESR signals at $g \approx 9.0$ (strong) and 2.0 (weak) at room temperature. The spectra of **1** and **2** are shown in Figure 4. Generally, observation of ESR signals of mononuclear six-coordinate manganese(III) complexes are often difficult because of the fast spin relaxation and large zero-field splitting.[32] However, when the coordination geometries around the manganese(III) ion are strongly distorted, the signals can be observed as anisotropic signals. In the present complexes, the geometries of manganese(III) ions have strong axial distortion along with weakly coordinated solvent molecules. In consequence, it is assumed that these strong anisotropic signals were observed at an apparent g value of about 9.0.[33] The weak signals at $g \approx 2.0$ might have arisen from manganese(II) impurities.

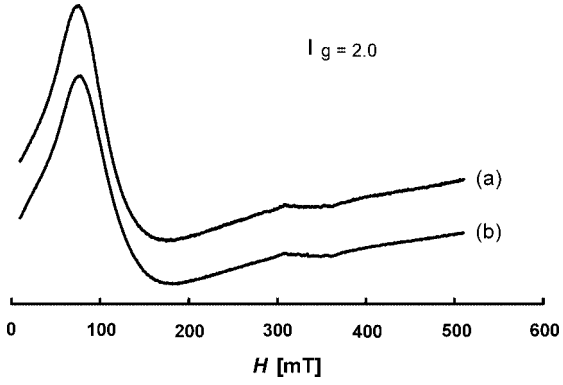

Figure 4. X-band polycrystalline ESR spectra of **1** (a) and **2** (b) at room temperature. The bar indicates the position of the weak resonance.

The magnetic moments per Mn atom of the complexes at room temperature are 4.90 (for **1**) and 4.83 (for **2**) B.M., which are close to the spin-only values (4.90) for four unpaired spins ($S = 2$). Magnetic susceptibility measurements for **1** were performed in the temperature range 2–300 K. The χ_A and μ_{eff} versus T plots are shown in Figure 5. The μ_{eff} values are virtually constant from 300 K to 50 K, and then rapidly decrease with decreasing temperature and reach 3.96 B.M. at 2 K. This behaviour indicates the presence of a very weak antiferromagnetic interaction between manganese(III) ions. The magnetic property was simulated by means of the triangular spin model for $S = 2$ (Scheme 3).

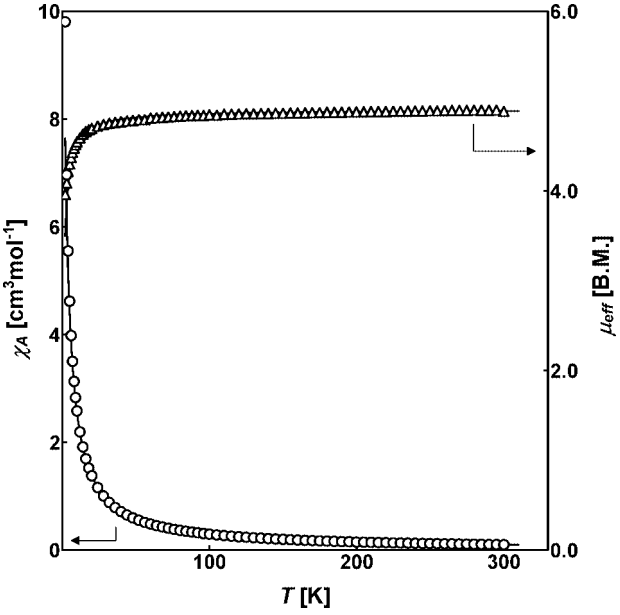

Figure 5. Temperature dependence of the magnetic susceptibilities for **1**. The solid curves were obtained as described in the text.

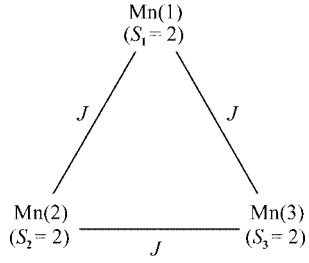

Scheme 3. Triangular spin model for **1**.

The Hamiltonian is written as in Equation (1).

$$H = -J(S_1S_2 + S_2S_3 + S_3S_1) \quad (1)$$

Magnetic susceptibilities are given by Equation (2), where χ_A is the magnetic susceptibility per manganese ion, and other symbols have their usual meanings.

$$\chi_A = \{Ng^2\beta^2/3k(T-\theta)\}\mathbf{A}/\mathbf{B} + N\alpha$$
$$\mathbf{A} = 182 + 220\exp(-12J/kT) + 180\exp(-22J/kT) + 112\exp(-30J/kT) + 50\exp(-36J/kT) + 6\exp(-40J/kT)$$
$$\mathbf{B} = 13 + 22\exp(-12J/kT) + 27\exp(-22J/kT) + 28\exp(-30J/kT) + 25\exp(-36J/kT) + 9\exp(-40J/kT) + \exp(-42J/kT) \quad (2)$$

The best fitting parameters are $J = -0.2$ cm^{-1}, $g = 2.00$, $N\alpha = 0$ and $\theta = -1.5$ K. For triangular complexes, spin-frustration behaviour was often observed. In the present complex **1**, the obtained J value suggests that the weak antiferromagnetic interactions are dominant. However, the absolute J value is too small to dispute the essence of magnetic interaction owing to the long Mn–Mn distances (av. 8.119 Å).

A notable result is the contribution of the θ value, which suggests that overall antiferromagnetic interactions are several times larger than the J value. As shown in the crystal packing diagram, **1** has a high-order structure linked through hydrogen bonds established between the coordinated methanol and the phenolic oxygen atom of neighbouring complex molecules. Such connections are known to mediate intermolecular magnetic interactions.[34–36] In addition, because the distance between the nearest intermolecular manganese ions, 5.7824(15) Å, is shorter than the intramolecular distances (av. 8.119 Å), it is assumed that the intermolecular antiferromagnetic interaction is larger than the intramolecular interaction.

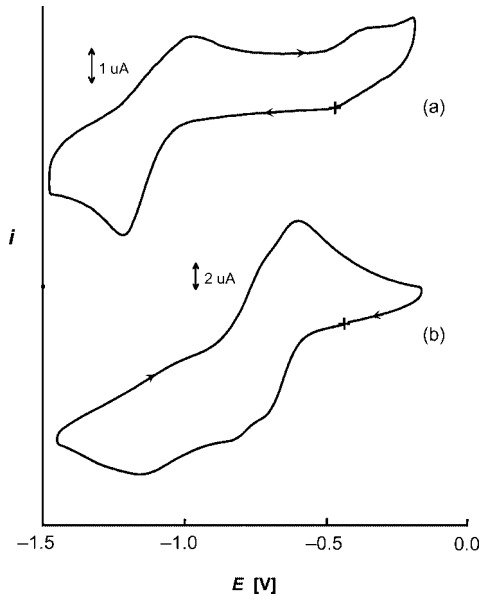

Figure 6. Cyclic voltammograms of H_3L^1 (a) and **1** (b); glassy-carbon electrode, scan rate 100 mV s^{-1}, concentration 1×10^{-3} M, in dmf.

Electrochemistry

Electrochemical properties of the present complexes were examined by cyclic voltammetry (CV) in dmf containing tbap (0.1 M) as the supporting electrolyte. The cyclic voltammograms of H_3L^1 and **1** are shown in Figure 6. When measurements were performed in the range from –0.1 to –1.4 V, three irreversible redox couples were observed at about –0.6, –0.7 and –1.0 V. The redox couples at about –1.0 V can be assigned to the reduction of the benzoxazole moiety, because the voltammogram of H_3L^1 also showed similar waves. In the positive range, both present complexes showed no wave except for the irreversible oxidation of phenolic oxygen atoms originating in the ligands. The electrochemical data of **1** and **2** are summarised in Table 3.

Although the first and second reduction waves are not so clear, it is assumed that they can be assigned to metal-centred one-electron transfer processes Mn_3(III,III,III)/Mn_3(II,III,III) and Mn_3(II,III,III)/Mn_3(II,II,III), respectively. The redox process of Mn_3(II,II,III)/Mn_3(II,II,II) could not be observed in the present measurements, even though we performed CV under various measurement conditions. It is considered that the effect of the ligand reduction process makes the voltammogram obscure. The potential differences (ΔE) between two metal-centred redox couples are higher than 36 mV, which is expected for a purely statistical treatment in the two-electron process.[37] In multinuclear complexes, ΔE values often increase when an electronic repulsion effect exists between the redox centres. In complex **1**, the bridging ligands forming long metal-to-metal distances are expected to yield small ΔE close to the statistical case. However, the ligands have a π-conjugation system that is expected to enhance the electronic communication between manganese ions. As a result, it is assumed that the electronic repulsion effect is enhanced in **1**; large ΔE values were observed in these complexes. Such a phenomenon was also observed in other macrocyclic complexes having long metal-to-metal distances like **1**.[1,38,39]

Table 3. Crystal data and collection details for H_3L^1, H_3L^2, H_4L' and complex **1**.

Compound	H_3L^1	H_3L^2	$H_4L'\cdot CH_3OH$	$\mathbf{1}\cdot 5CH_3OH\cdot 3H_2O$
Empirical formula	$C_{20}H_{14}N_2O_4$	$C_{28}H_{18}N_2O_4$	$C_{21}H_{20}N_2O_5$	$C_{68}H_{71}Mn_3N_6O_{23}$
Formula mass	346.34	446.46	380.40	1505.15
Crystal size [mm]	0.20 × 0.20 × 0.20	0.48 × 0.10 × 0.02	0.60 × 0.20 × 0.10	0.40 × 0.40 × 0.30
Crystal system	monoclinic	monoclinic	monoclinic	monoclinic
Space group	$P2_1/n$ (#14)	$P2_1/n$ (#14)	$P2_1/c$ (#14)	$P2_1/c$ (#14)
a [Å]	11.505(7)	17.994(9)	13.658(5)	12.241(6)
b [Å]	9.706(4)	6.220(5) Å	6.179(4)	16.556(7)
c [Å]	14.608(4)	20.333(14)	22.706(5)	36.278(8)
β [°]	103.55(4)	111.52(3)	103.52(2)	93.44(4)
V [Å^3]	1585.8(13)	2116.9(23)	1863.1(15)	7339.0(48)
Z	4	4	4	4
$D_{calcd.}$ [g cm^{-3}]	1.451	1.401	1.356	1.362
F(000)	720.00	928.00	800	3120.00
μ(Mo-K_α) [cm^{-1}]	1.028	0.948	0.977	5.857
Number of unique reflections	3627 (R_{int} = 0.097)	2198 (R_{int} = 0.163)	3542 (R_{int} = 0.042)	13346 (R_{int} = 0.041)
Number of observations	3627	2198	3542	13346
Number of variables	237	308	254	902
R ($I > 2\sigma$), Rw (all data)	0.0699, 0.1575	0.0568, 0.1450	0.0553, 0.1983	0.0685, 0.2550

Conclusions

In the present study, it was demonstrated that the newly obtained unsymmetrical pentadentate ligands H_3L^1 and H_3L^2 support the formation of trinuclear manganese(III) complexes described as $[Mn_3(L^n)_3(solvent)_3]$. In the present complexes, the manganese atoms have six-coordinate geometries with elongated octahedral distortion. The molecular structures of the complexes are regarded as tripodal pyramids with a small cavity. The cavity is used for π–π stacking between enantiomer pairs. The magnetic interactions among trinuclear metal cores are very weak because of the long metal-to-metal distances. It is interesting that the obtained complexes are not phenoxo-bridged dinuclear complexes but trinuclear complexes. The result suggests that the present ligands can provide new applications for obtaining trinuclear macrocyclic complexes and can develop the understanding of self-assembly.

Experimental Section

Materials: All ordinary reagents and solvents were purchased and used as received, unless otherwise noted. Methanol was purified by distillation from magnesium turnings.

Preparations

H_4L'·HCl: A solution of 2-hydroxybenzaldehyde (0.976 g, 8 mmol) in dry methanol (10 mL) was added dropwise to a solution of 4,6-diaminoresorcinol dihydrochloride (0.852 g, 4 mmol) in dry methanol (40 mL) with stirring. The solution became a bright red suspension. The resulting precipitate was filtered off, washed with dry methanol and dried in vacuo. Yield of H_4L'·HCl·2H_2O: 1.36 g, 81%. $C_{20}H_{21}ClN_2O_6$ (420.85): calcd. C 57.08, H 5.03 N, 6.66; found C 56.76, H 5.04, N 6.77. IR (KBr): $\tilde{\nu}$ = 3355 and 3070 (OH), 1622–1651 (C=N), 860 and 758 (phenyl) cm^{-1}. ^1H NMR (300 MHz, dmso, tms): δ = 9.12 (s, 2 H), 7.80 (s, 1 H), 7.62 (d, 2 H), 7.45–7.39 (t, 2 H), 7.02–6.92 (m, 4 H), 6.72 (s, 1 H) ppm. FAB-MS: *m*/*z* = 349.1 [(H_4L')H^+].

H_4L': A solution of 2-hydroxybenzaldehyde (0.976 g, 8 mmol) in dry methanol (10 mL) was added dropwise to a solution of 4,6-diaminoresorcinol dihydrochloride (0.852 g, 4 mmol) in dry methanol (40 mL) with stirring. The solution became a bright red suspension. A solution of triethylamine (0.808 g, 8 mmol) in dry methanol (5 mL) was added slowly, and the mixture was stirred at room temperature for 1 h. The resulting orange precipitate was filtered off, washed with dry methanol and dried in vacuo. Single crystals suitable for X-ray crystallography were obtained by recrystallisation from dmf solution layered with methanol. Yield of H_4L'·1/2MeOH·1/2H_2O: 1.143 g, 77%. $C_{20.5}H_{19}N_2O_5$ (373.39): calcd. C 65.94, H 5.13, N 7.50; found C 65.66, H 5.19, N 7.45. IR (KBr): $\tilde{\nu}$ = 1615–1634 (C=N), 859 and 756 (phenyl) cm^{-1}. ^1H NMR (300 MHz, dmso, tms): δ = 9.03 (s, 2 H), 7.65 (s, 1 H), 7.60 (d, 2 H), 7.35 (t, 2 H), 6.97–6.91 (m, 4 H), 6.65 (s, 1 H) ppm.

H_3L^1: The next day, ligand H_3L^1 precipitated from the orange solution from which the ligand H_4L' had been filtered off. Single crystals suitable for X-ray crystallography were obtained by recrystallisation from dmf solution layered with acetonitrile. Yield of H_3L^1·4H_2O: 0.013 g, 0.8%. $C_{20}H_{22}N_2O_8$ (418.40): calcd. C 57.41, H 5.30, N 6.70; found C 57.27, H 5.19, N 6.78. IR (KBr): $\tilde{\nu}$ = 3202 (OH), 1615–1634 (C=N), 765 and 750 (phenyl) cm^{-1}. ^1H NMR (300 MHz, dmso, tms): δ = 9.07 (s, 1 H), 7.99 (d, 1 H), 7.91 (s, 1 H), 7.64 (d, 1 H), 7.51 (t, 1 H), 7.41 (t, 1 H), 7.34 (s, 1 H), 7.12 (d, 1 H), 7.07 (d, 1 H), 6.98 (t, 2 H) ppm. FAB-MS: *m*/*z* = 347.2 [(H_3L^1)H^+].

H_3L^2: A solution of triethylamine (0.808 g, 8 mmol) in dry 1,4-dioxane (10 mL) was added dropwise to a solution of 4,6-diaminoresorcinol dihydrochloride (0.852 g, 4 mmol) and 2-hydroxy-1-naphthaldehyde (1.376 g, 8 mmol) in dry 1,4-dioxane (30 mL) with stirring. The dark green slurry was stirred at room temperature for 3 h. The resulting precipitate was filtered off and washed with dry 1,4-dioxane. Upon recrystallisation from a mixed solution of dmf/methanol, H_3L^2 precipitated as orange needles, was filtered off, and dried in vacuo. Single crystals suitable for X-ray crystallography were obtained by recrystallisation from dmf solution layered with methanol. Yield of H_3L^2·1/2H_2O: 0.27 g, 14.8%. $C_{28}H_{19}N_2O_{4.5}$ (455.47): calcd. C 73.84, H 4.20, N 6.15; found C 73.46, H 4.54, N 6.47. IR (KBr): $\tilde{\nu}$ = 3238 (OH), 1615–1622 (C=N), 746 (phenyl) cm^{-1}. ^1H NMR (300 MHz, dmso, tms): δ = 9.67 (s, 1 H), 8.58–8.51 (m, 3 H), 8.08 (d, 1 H), 7.96 (d, 1 H), 7.84 (d, 1 H), 7.71 (d, 1 H), 7.64 (t, 1 H), 7.54–7.44 (m, 3 H), 7.37 (d, 1 H), 7.30 (t, 1 H), 6.84 (d, 1 H) ppm. FAB-MS: *m*/*z* = 447.2 [(H_3L^2)H^+].

$[Mn_3(L^1)_3(CH_3OH)_3]$ (1): A methanol solution (5 mL) of triethylamine (0.020 g, 0.2 mmol) was added to an orange suspension of H_4L'·HCl (0.077 g, 0.2 mmol) in methanol (15 mL) with stirring. A solution of manganese(II) acetate tetrahydrate (0.049 g, 0.2 mmol) in dry methanol (20 mL) was added to the resulting light brown solution, and the mixture was stirred for 10 min. The obtained dark brown solution was filtered, and the filtrate was allowed to stand at room temperature for 1 d to give dark brown crystals suitable for X-ray crystallography. Yield of **1**: 0.039 g, 45.3%. $C_{63}H_{45}Mn_3N_6O_{15}$ (1290.90): calcd. C 58.62, H 3.51, Mn 12.77, N 6.51; found C 58.47, H 3.10, Mn 13.07, N 6.74. IR (KBr): $\tilde{\nu}$ = 1606 (C=N), 1146 (C–O), 752 (phenyl) cm^{-1}. UV (dmf): λ (ε) = 373 (37200), 503 (22900) and 800 sh (500 $dm^3 mol^{-1} cm^{-1}$) nm. Λ_m (dmf) = 2.60 $S cm^{-2} mol^{-1}$.

$[Mn_3(L^2)_3(dmf)(CH_3OH)(H_2O)]$ (2): A solution of manganese(II) acetate tetrahydrate (0.025 g, 0.1 mmol) in dry methanol (10 mL) was added to an orange suspension of H_3L^2 (0.045 g, 0.1 mmol) in dmf (10 mL). The resulting dark brown mixture was stirred for 3 h and then filtered to remove insoluble materials. Triethylamine (0.02 g, 0.2 mmol) was added to the filtrate, and the solution was allowed to stand at room temperature for 3 d to give dark brown crystals suitable for X-ray crystallography. Yield of **2**·2dmf·CH_3OH: 0.029 g, 48.4%. $C_{95}H_{76}Mn_3N_9O_{18}$ (1796.51): calcd. C 63.51. H 4.26, Mn 9.17, N 7.02; found C 63.21, H 3.94, Mn 8.80, N 6.96. IR (KBr): $\tilde{\nu}$ = 1616, 1600 (C=N), 1144 (C–O), 828 and 756 (phenyl) cm^{-1}. UV (dmf): λ (ε) = 410 sh (31600), 465 sh (20000), 526 sh (19900), 769 sh (1000) and 870 sh (500 $dm^3 mol^{-1} cm^{-1}$) nm. Λ_m (dmf) = 1.90 $S cm^{-2} mol^{-1}$.

Physical Measurements: Elemental analyses for C, H and N were obtained at the Elemental Analysis Service Center, Kyushu University. Manganese was determined with a Perkin–Elmer A Analyst 100 atomic absorption spectrometer. Nuclear magnetic resonance spectra were recorded with a JNM-AL300 spectrometer in [D_6]-dmso using tetramethylsilane as the internal standard. FAB mass spectra for H_3L^n and H_4L' were recorded with a JMS-GC mate II. Infrared spectra and electronic spectra were recorded with a Perkin–Elmer Spectrum 2000 FTIR spectrometer on KBr disks and a Perkin–Elmer Lambda 19 UV/Vis/NIR spectrophotometer, respectively, at the Instrumental Analysis Center, Saga University. X-band ESR spectra were recorded with a JEOL JES-TE300 ESR spectrometer at room temperature. Magnetic susceptibilities in the temperature range 2–300 K were measured with a Quantum Design

MPMS XL SQUID susceptometer under an applied magnetic field of 500 G. The susceptibilities at room temperature were determined by the Gouy method with a Sherwood Scientific Magnetic Susceptibility Balance. These were corrected for the diamagnetism of the constituent atoms using Pascal's constant.[40] The effective magnetic moments were calculated from the equation $\mu_{eff} = 2.828[(\chi_A - N\alpha)T]^{1/2}$, where χ_α is the atomic magnetic susceptibility and $N\alpha$ is the temperature-independent paramagnetism. Molar conductances were determined in dmf at 25 °C with a TOA EC METER CM-30G. Cyclic voltammograms (CVs) were obtained with a BAS 100B electrochemical voltammetric analyser. The CV measurements were carried out in dmf containing 0.1 M tetrabutylammonium perchlorate (tbap) as supporting electrolyte. (***Caution:*** tbap is explosive and should be handled with great care!) The three-electrode cell that was used was equipped with a glassy carbon (ϕ = 3 mm) working electrode, a platinum wire counter electrode, and an Ag/Ag^+ electrode as the reference.

X-ray Crystal Structure Determinations: The diffraction data were measured with a Rigaku AFC5S automated four-circle diffractometer having graphite-monochromated Mo-K_α (λ = 0.71069 Å) radiation. Cell constants and an orientation matrix for data collection were obtained from a least-squares refinement using the setting angles of 25 carefully centered reflections for complexes **1**, 24 reflections for H_3L^1 and H_4L', and 6 reflections for H_3L^2. The data were collected using the ω-scan technique to a maximum 2θ value of 55.1° for H_3L^1, 55.0° for H_4L' and **1**, and the ω-2θ-scan technique to a maximum 2θ value of 45.0° for H_3L^2. The weak reflections [$I < 10\sigma(I)$] were rescanned (maximum 5 rescans) and the counts were accumulated to assure good counting statistics. Stationary background counts were recorded on each side of the reflection. The ratio of the peak counting time was 2:1. The intensities of three representative reflections were measured after every 150 reflections. Over the course of data collections, the standards decreased by 0.7% for **1**. Polynomial correction factors were applied to the data to account for this phenomenon. Empirical absorption corrections, based on azimuthal scans of several reflections, were applied. The data were corrected for Lorentz and polarisation effects. The crystallographic data and collection details are summarised in Table 3. The structures were solved by direct methods (SIR92) and expanded using Fourier techniques.[41,42] All hydrogen atoms were located in the calculated positions and refined using the riding model. The final cycle of full-matrix least-squares refinement on F using SHELXL-97 was based on observed reflections and variable parameters, and converged with unweighted and weighted agreement factors of R and R_w.[43,44] Neutral atom scattering factors were taken from Cromer and Waber.[45] Anomalous dispersion effects were included in F_c;[46] the values for $\Delta f'$ and $\Delta f''$ were those of Creagh and McAuley.[47,48] All calculations were performed using the Rigaku CrystalStructure crystallographic software package, except for refinement, which was performed using SHELXL-97.[49] CCDC-625063 to -625066 contain the supplementary crystallographic data for this paper. These data can be obtained free of charge from The Cambridge Crystallographic Data Centre via www.ccdc.cam.ac.uk/data_request/cif.

Supporting Information (see footnote on the first page of this article): Packing diagram showing hydrogen bonding in complex **1** (Figure S1), ORTEP drawing of complex **2** (Figure S2).

Acknowledgments

This work was supported by a Grant-in-Aid for Science Research (C) (No. 15510092) and the "Nanotechnology Support Project" of the Ministry of Education, Science, Sports and Culture of Japan.

[1] K. Severin, *Coord. Chem. Rev.* **2003**, *245*, 3–10.
[2] M. Murugesu, J. Raftery, W. Wernsdorfer, G. Christou, E. K. Brechin, *Inorg. Chem.* **2004**, *43*, 4203–4209.
[3] R. H. Fish, *Coord. Chem. Rev.* **1999**, *185–186*, 569–584.
[4] R. Wang, M. Hong, J. Luo, R. Cao, J. Weng, *Chem. Commun.* **2003**, 1018–1019.
[5] D. Moon, M. S. Lah, *Inorg. Chem.* **2005**, *44*, 1934–1940.
[6] M. Consiglo, F. Maggio, T. Pizzino, V. Romano, *Inorg. Nucl. Lett.* **1978**, *14*, 135–137.
[7] a) H. Ōkawa, M. Nakamura, S. Kida, *Bull. Chem. Soc. Jpn.* **1982**, *55*, 466–470; b) W. Kanda, M. Nakamura, H. Ōkawa, S. Kida, *Bull. Chem. Soc. Jpn.* **1983**, *56*, 744–747.
[8] H. Asada, M. Ozeki, M. Fujiwara, T. Matsushita, *Polyhedron* **2002**, *21*, 1139–1148.
[9] a) J. Qiao, L. D. Wang, L. Duan, Y. Li, D. Q. Zhang, Y. Qiu, *Inorg. Chem.* **2004**, *43*, 5096–5102; b) J. Qiao, L. D. Wang, J. F. Xie, G. T. Lei, G. S. Wu, Y. Qiu, *Chem. Commun.* **2005**, 4560–4562.
[10] S. Dutta, P. Basu, A. Chakravorty, *Inorg. Chem.* **1991**, *30*, 4031–4037.
[11] a) X. Chen, F. J. Femia, J. W. Babich, J. Zubieta, *Inorg. Chim. Acta* **2000**, *308*, 80–90; b) X. Chen, F. J. Femia, J. W. Babich, J. Zubieta, *Inorg. Chim. Acta* **2001**, *316*, 33–40.
[12] M. Mikuriya, N. Torihara, H. Ōkawa, S. Kida, *Bull. Chem. Soc. Jpn.* **1981**, *54*, 1063–1067.
[13] D. P. Kessissoglou, X. Li, W. M. Butler, V. L. Pecoraro, *Inorg. Chem.* **1987**, *26*, 2487–2492.
[14] M. Koikawa, H. Ōkawa, S. Kida, *J. Chem. Soc. Dalton Trans.* **1988**, 641–645.
[15] S. K. Chandra, P. Basu, D. Ray, S. Pal, A. Chakravorty, *Inorg. Chem.* **1990**, *29*, 2423–2428.
[16] M. Mikuriya, D. Jie, Y. Kakuta, T. Tokii, *Bull. Chem. Soc. Jpn.* **1993**, *66*, 1132–1139.
[17] H. Asada, M. Ozeki, M. Fujiwara, T. Matsushita, *Chem. Lett.* **1999**, 525–526.
[18] a) A. Elmali, I. Svoboda, *Z. Naturforsch., B: Chem. Sci.* **2001**, *56*, 897–900; b) A. Elmali, Y. Elerman, C. T. Zeyrek, I. Svoboda, *Z. Naturforsch., B: Chem. Sci.* **2003**, *58*, 433–437.
[19] P. A. N. Reddy, M. Nethaji, A. R. Chakravarty, *Eur. J. Inorg. Chem.* **2003**, 2318–2324.
[20] R. Kannappan, D. M. Tooke, A. L. Spek, J. Reedijk, *Inorg. Chim. Acta* **2006**, *359*, 334–338.
[21] E. Lambert, B. Chabut, S. Chardon-Noblat, A. Deronzier, G. Chottard, A. Bousseksou, J.-P. Tuchagues, J. Laugier, M. Bardet, J.-M. Latour, *J. Am. Chem. Soc.* **1997**, *119*, 9424–9437.
[22] D. E. Fenton, *Chem. Soc. Rev.* **1999**, *28*, 159–168.
[23] C. Belle, J.-L. Pierre, *Eur. J. Inorg. Chem.* **2003**, 4137–4146.
[24] G. Manecke, W. E. Wille, *Makromol. Chem.* **1970**, *133*, 61–82.
[25] a) Y. Kurusu, W. Storck, G. Manecke, *Makromol. Chem.* **1975**, *176*, 3185–3200; b) Y. Kurusu, *Macromol. Symp.* **1996**, *105*, 173–177.
[26] O. Waldmann, J. Massmann, P. Müller, G. S. Hanan, D. Volkmer, U. S. Schubert, J.-M. Lehn, *Phys. Rev. Lett.* **1997**, *78*, 3390–3393.
[27] L. Zhao, C. J. Matthews, L. K. Thompson, S. L. Heath, *Chem. Commun.* **2000**, 265–266.
[28] C. E. Hulme, M. Watkinson, M. Haynes, R. G. Pritchard, C. A. McAuliffe, N. Jaiboon, B. Beagley, A. Sousa, M. R. Bermejo, M. Fondo, *J. Chem. Soc. Dalton Trans.* **1997**, 1805–1814.
[29] C. Palopoli, M. González-Sierra, G. Robles, F. Dahan, J.-P. Tuchagues, S. Signorella, *J. Chem. Soc. Dalton Trans.* **2002**, 3813–3819.
[30] C. Boskovic, E. Rusanov, H. Stoeckli-Evans, H. U. Güdel, *Inorg. Chem. Commun.* **2002**, *5*, 881–886.
[31] N. Hoshino, T. Ito, M. Nihei, H. Oshio, *Inorg. Chem. Commun.* **2003**, *6*, 377–380.

[32] S. L. Dexheimer, J. W. Gohdes, M. K. Chan, K. S. Hagen, W. H. Armstrong, M. P. Klein, *J. Am. Chem. Soc.* **1989**, *111*, 8923–8925.
[33] K. P. Bryliakov, D. E. Babushkin, E. P. Talsi, *J. Mol. Catal. A* **2000**, *158*, 19–35.
[34] G. D. Munno, W. Ventura, G. Viau, F. Lloret, J. Faus, M. Julve, *Inorg. Chem.* **1998**, *37*, 1458–1464.
[35] C. Desplanches, E. Ruiz, A. Rodríguez-Fortea, S. Alvarez, *J. Am. Chem. Soc.* **2002**, *124*, 5197–5205.
[36] a) R. Karmakar, C. R. Choudhury, G. Bravic, J.-P. Sutter, S. Mitra, *Polyhedron* **2004**, *23*, 949–954; b) M. S. Ray, A. Ghosh, R. Bhattacharya, G. Mukhopadhyay, M. G. B. Drew, J. Ribas, *Dalton Trans.* **2004**, 252–259.
[37] G. D. Santis, L. Fabbrizzi, M. Licchelli, P. Pallavicini, *Coord. Chem. Rev.* **1992**, *120*, 237–257.
[38] N. Shan, S. J. Vickers, H. Adams, M. D. Ward, J. A. Thomas, *Angew. Chem. Int. Ed.* **2004**, *43*, 3938–3941.
[39] L. A. Berben, M. C. Faia, N. R. M. Crawford, J. R. Long, *Inorg. Chem.* **2006**, *45*, 6378–6386.
[40] Landoldt-Börnstein, Neue Serie II/11, Springer-Verlag, Berlin, **1981**.
[41] SIR92: A. Altomare, G. Cascarano, C. Giacovazzo, A. Guagliardi, M. Burla, G. Polidori, M. Camalli, *J. Appl. Crystallogr.* **1994**, *27*, 435.
[42] *DIRDIF99*: P. T. Beurskens, G. Admiraal, G. Beurskens, W. P. Bosman, R. de Gelder, R. Israel, J. M. M. Smits, *The DIRDIF-99 program system*, Technical Report of the Crystallography Laboratory, University of Nijmegen, The Netherlands, **1999**.
[43] $R = \Sigma||F_o| - |F_c||/\Sigma|F_o|$, $Rw = \{\Sigma[w(F_o^2 - F_c^2)^2]/\Sigma w(F_o^2)^2\}^{1/2}$ where w = least-squares weights.
[44] G. M. Sheldrick, *SHELX97*, **1997**.
[45] D. T. Cromer, J. T. Waber (Eds.), *International Tables for X-ray Crystallography*, Kynoch Press, Birmingham, **1974**, vol. IV.
[46] J. A. Ibers, W. C. Hamilton, *Acta Crystallogr.* **1964**, *17*, 781.
[47] D. C. Creagh, W. J. McAuley in *International Tables for Crystallography* (Ed.: A. J. C. Wilson), Kluwer Academic Publishers, Boston, **1992**, vol. C, pp. 219–222.
[48] D. C. Creagh, J. H. Hubbell in *International Tables for Crystallography* (Ed.: A. J. C. Wilson), Kluwer Academic Publishers, Boston, **1992**, vol. C, pp. 200–206.
[49] *CrystalStructure 3.7.0*, Crystal Structure Analysis Package, Rigaku, Rigaku/MSC, **2000**–**2005**.

Received: January 18, 2007
Published Online: June 25, 2007

